University of Sistan and Baluchestan

Challenges in Nano and Micro Scale Science and Technology

Online ISSN: 2821 - 000X

Numerical Study of the Effect of Urine Presence and Convection on Magnetic Nanoparticle Hyperthermia in the Treatment of Bladder Cancer

Sahar Marami[1] | Mohammad Hossein Tavakoli[2] | Abdolazim Sedighi Pashaki[3] | Safoora Nikzad[4]

1. Department of Physics, Faculty of Science, Bu-Ali Sina University, Hamedan, Iran
2. Corresponding Author, Department of Physics, Faculty of Science, Bu-Ali Sina University, Hamedan, Iran. Email: mht@basu.ac.ir
3. Cancer Research Center, Hamadan University of Medical Sciences, Hamedan, Iran
4. Department of Medical Physics, Faculty of Medicine, Isfahan University of Medical Sciences, Isfahan, Iran

Article Info

Article type:
Research Article

Keywords:
bladder cancer,
fluid modeling,
heat transfer,
hyperthermia,
magnetic nanoparticles

ABSTRACT

Magnetic nanoparticle hyperthermia is a preclinical treatment for bladder cancer that employs ferromagnetic nanoparticles exposed to an external alternating magnetic field to elevate the temperature within the tumor. In this study, magnetic hyperthermia using Fe_3O_4 nanoparticles was simulated for T1 non-muscle-invasive bladder cancer and T2 muscle-invasive bladder cancer, investigating the effect of the presence of urine and its convection within the bladder in this treatment method. For this purpose, simulations for both stages of bladder cancer were conducted for three cases. First, the bladder without urine was modeled as a homogeneous muscle tissue. Next, to investigate the effect of the absence of perfusion, the bladder containing urine was modeled, but the effect of convection was neglected. Finally, the bladder containing urine was modeled, incorporating the effect of convection. The distribution of the volumetric heat generation rate due to induction heating, the volumetric power dissipation of the magnetic nanoparticles, and the temperature are presented for three simulation cases and two stages of bladder cancer. Pennes and Navier-Stokes equations were used to obtain the temperature distribution in solid tissues and fluid, respectively. The equations were solved using the finite element method in two dimensions. The results demonstrate that in magnetic nanoparticle hyperthermia, convection within urine increases heat generation, reduces temperature, and creates a non-uniform temperature distribution in the tumor for both stages of bladder cancer. Additionally, the more uniform temperature distribution in T1 compared to T2 suggests that this treatment is more effective for non-muscle-invasive bladder cancer than for muscle-invasive bladder cancer.

1. INTRODUCTION

Bladder cancer is one of the most prevalent cancers, particularly among men. More than 90 % of bladder cancers originate in the mucosal layer, the innermost lining of the bladder wall, and are classified as urothelial cell carcinoma (UCC). Bladder cancer is classified into two types based on the extent of its spread: non-muscle-invasive bladder cancer (NMIBC), which is confined to the inner lining of the bladder, and muscle-invasive bladder cancer (MIBC), which invades the muscular layer of the bladder wall and may extend to surrounding tissues.

These two types of bladder cancer require distinct treatment approaches. Hyperthermia in bladder cancer involves elevating the temperature of the tumor to approximately 41–44 °C, serving as an adjuvant therapy for this condition [1,2]. Currently, hyperthermia is used in the treatment of NMIBC in combination with chemotherapy, utilizing drugs such as mitomycin C (MMC). Hyperthermia enhances the absorption of this drug within tumor cells [3–5]. Additionally, hyperthermia, in combination with radiotherapy and systemic chemotherapy, may serve as an alternative to radical cystectomy in the treatment of MIBC [6–8].

In hyperthermia, longer treatment durations and higher tumor temperatures lead to increased tumor destruction. However, this can lead to a rise in temperature in the surrounding tissues, damaging healthy tissue as well. Therefore, challenges associated with hyperthermia methods include heterogeneous temperature distribution, excessive temperature elevation in the tumor, and

How to Cite this paper: Marami S. Tavakoli M.H. Sedighi Pashaki A. Nikzad S. Numerical Study of the Effect of Urine Presence and Convection on Magnetic Nanoparticle Hyperthermia in the Treatment of Bladder Cancer. *Challenges in Nano and Micro Scale Science and Technology*. 2024; 12(2): 30-40. DOI: 10.22111/cnmst.2025.52873.1266

© Marami S. Tavakoli M.H. Sedighi Pashaki A. Nikzad S. Publisher: University of Sistan and Baluchestan.

DOI: 10.22111/cnmst.2025.52873.1266

unintended temperature increases in healthy tissues [9]. Consequently, the goal is to achieve the highest possible temperature within the tumor while avoiding pain or thermal toxicity, which typically occurs at temperatures exceeding 45 °C [10,11].

One of the preclinical hyperthermia approaches for bladder cancer involves heating the tumor using ferromagnetic nanoparticles exposed to an external alternating magnetic field (AMF). In this method, the nanoparticles are delivered either directly or systemically, aiming to achieve high concentrations within the tumor, and are subsequently exposed to an externally applied AMF [1]. The primary advantage of this method lies in the ability to accumulate nanoparticles as thermal mediators within the tumor, creating a targeted temperature difference between the tumor and the surrounding healthy tissue. As a result, this method enables the generation of concentrated heat within the tumor [9]. Oliveira et al. were the first to investigate, in a preclinical study, the feasibility of using magnetic fluid hyperthermia and the potential for localizing heat within the rat bladder. In this study, iron oxide nanoparticles were used in combination with an AMF at a frequency of 40 kHz. They elevated the bladder temperature to the target temperature of 42 °C in under 10 minutes. This study demonstrated that the magnetic nanofluid hyperthermia method effectively generates concentrated heat within the rat bladder while minimizing heat in the surrounding tissues [12].

Yuan et al. were the first to investigate convective heat transfer in the bladder through a clinical trial. They introduced a novel treatment planning method and demonstrated its potential to enhance treatment quality. In this study, a combination of chemotherapy and radiofrequency (RF)-induced hyperthermia was utilized for the treatment of NMIBC [13]. Sadee and Kashdan conducted the first quantitative analysis of chemo-thermotherapy by developing a mathematical model. In this study, the necessary heat was generated using an intravesical microwave antenna system. They demonstrated that chemo-thermotherapy using this method can result in local hot spots, potentially causing burns in areas of the bladder and surrounding tissues. Additionally, they found that the presence of residual urine or a saline solution in the bladder leads to excessive but ineffective heating of the bladder wall, preventing the desired depth of heat penetration. This outcome is qualitatively similar to heating the solution externally and circulating it within the bladder cavity. Therefore, continuous monitoring of the solution's salinity is essential to prevent ineffective heating and the formation of local hot spots [14]. To improve the accuracy of treatment planning in NMIBC hyperthermia using RF, Schooneveldt et al. compared the results of three models: the common muscle-like solid bladder model, the static bladder contents model (without fluid dynamics), and the dynamic bladder contents model (with fluid dynamics), against the measured temperature values during treatment. The dynamic model achieved significantly higher and more uniform bladder temperatures compared to the previously used muscle-like model. The results of this study demonstrated that the dynamic model's temperature predictions exhibited less deviation from the measured temperature values during treatment compared to the other two models, offering a more accurate representation of clinical conditions [2]. Additionally, Ooi et al. investigated the impact of natural convection on gold nanorods-assisted photothermal therapy for bladder cancer in mice. They observed that natural convection currents in urine exert a cooling effect. Therefore, natural convection within the bladder at low heating levels may dissipate heat from the targeted tissue, potentially compromising treatment effectiveness. Conversely, at high heating levels, cooling may help prevent excessive thermal damage to surrounding tissues [15].

Realistic bladder modeling plays a critical role in optimizing hyperthermia treatment for bladder cancer. However, hyperthermia treatment planning systems do not model fluid dynamics in the bladder lumen, modeling it as a solid instead of a fluid [2]. Given the presence of urine within the bladder during treatment, it is essential to account for convection effects in all hyperthermia methods to develop a more accurate bladder model. In this study, we investigated the impact of urine and its convection on magnetic nanoparticle (MNP) hyperthermia in two stages of bladder cancer (T1 and T2). The stages of bladder cancer are schematically illustrated in Figure 1. The required heat is generated by untargeted Fe_3O_4 MNPs localized within the tumor, under the influence of an external AMF produced by an induction coil positioned around the patient. To examine the effects of urine and its convection, three models were developed for both T1 and T2 stages: first, a common solid, muscle-like bladder model without urine; second, a bladder model with urine but without convection; and finally, a bladder model with urine incorporating convection. By comparing the results of these three models, the influence of urine presence and its convective flow on MNP hyperthermia performance was evaluated.

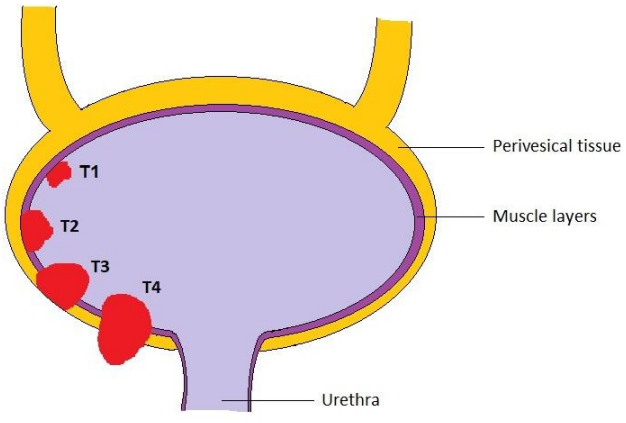

Fig. 1. A schematic diagram of the bladder and the stages of bladder cancer: T1 (the tumor remains within the bladder's inner lining), T2 (the tumor invades the muscle wall of the bladder), T3 (the tumor spreads to the perivesical tissue), and T4 (the tumor metastasizes to surrounding organs).

2. METHODS

2.1. Geometrical Model and Assumptions

The problem investigated in this study is modeled as two-dimensional (2D). The system is assumed to exhibit rotational (cylindrical) symmetry about the z-axis, implying that all variables are independent of the azimuthal coordinate. The geometry, illustrated in Figure 2, includes an induction coil, the pelvis, the bladder, and a spherical tumor embedded in the bladder wall.

Untargeted Fe_3O_4 MNPs are assumed to accumulate within the tumor and be uniformly distributed throughout its volume. When exposed to the AMF generated by the coil, these nanoparticles act as localized heat sources. The following key assumptions underlie the modeling approach:

- Cylindrical symmetry about the z-axis.
- All materials, except MNPs, are isotropic, non-magnetic, and electrically neutral.
- Nanoparticles are uniformly distributed within the tumor.
- Steady-state conditions prevail.

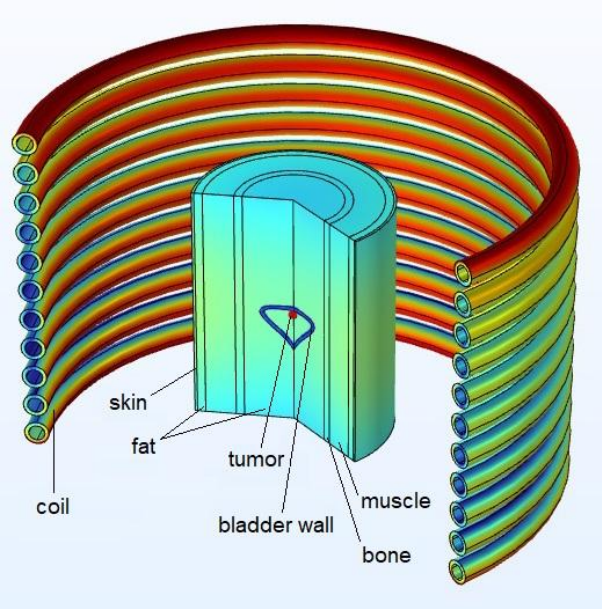

Fig 2. The geometry considered in the hyperthermia process.

2.2. Induction Heating

Passing an alternating current (AC) through the coil generates a time-varying magnetic field (in accordance with Ampere's law), which in turn induces an electric field around the coil (as described by Faraday's law). When electrically conductive materials (such as the human body) are placed within this field, eddy currents are induced in these materials. Due to the electrical resistance of the materials, Joule heating (RI^2) occurs.

By solving Maxwell's equations and employing the relationship between the vector potential and the magnetic field $\left(\vec{B} = \nabla \times \vec{A}\right)$, along with the principles of Joule heating, the heat generated in the tissue can be expressed as:

$$Q = \frac{|-i\omega\sigma A_0|^2}{2\sigma} \tag{1}$$

where ω represents the angular frequency, σ is the electrical conductivity of the tissue, and A_0 denotes the complex amplitude of the vector potential [16].

2.3. The Power Dissipation of MNPs

The volumetric power dissipation of MNPs is described as:

$$P = \mu_0 \pi \chi_0 H_0^2 f \frac{2\pi f\tau}{1+(2\pi f\tau)^2} \tag{2}$$

where $\mu_0 = 4\pi \times 10^{-7}$ is the permeability of free space, χ_0 is the equilibrium susceptibility, H_0 and f are the amplitude and the frequency of AMF, respectively, and τ is the effective relaxation time given by:

$$\tau = \frac{\tau_B \tau_N}{\tau_B + \tau_N} \tag{3}$$

where τ_B and τ_N are the Brownian and the Néel relaxation times, respectively, and τ_B is given by the following relationship:

$$\tau_B = \frac{3\eta V_H}{k_B T} \tag{4}$$

where η is the viscosity of the medium, k_B is the Boltzmann constant, and T is the absolute temperature. V_H represents the hydrodynamic volume of the MNPs, defined as $V_H = \frac{\pi(D+2\delta)^3}{6}$, where, D is the diameter of the MNPs and δ is the thickness of the ligand layer. The Néel relaxation time, τ_N, is expressed as follows:

$$\tau_N = \frac{\sqrt{\pi}}{2}\tau_0 \frac{e^{\Gamma}}{\sqrt{\Gamma}} \tag{5}$$

where τ_0 is the average relaxation time in response to thermal fluctuations, typically assumed to be $\tau_0 = 10^{-9}s$. Here, $\Gamma = \frac{K_{eff}V_M}{k_B T}$ where K_{eff} is the effective anisotropy constant, and V_M is the volume of the MNP. The equilibrium susceptibility, χ_0, is described as:

$$\chi_0 = \chi_i \frac{3}{\xi}\left(coth\,\xi - \frac{1}{\xi}\right) \tag{6}$$

where $\chi_i = \frac{\mu_0 \phi M_d^2 V_M}{3} k_B T$ is the initial susceptibility, and $\xi = \frac{\mu_0 M_d H V_M}{k_B T}$ is the Langevin parameter. ϕ represents the volume fraction of MNPs, and M_d is the domain magnetization [17].

2.4. Heat Transfer in Solid Tissues

The temperature distribution in the tissue and tumor (modeled as solid tissues) is obtained using the Pennes bioheat equation, given by the following relations, respectively [18]:

$$\rho_1 c_1 \frac{\partial T}{\partial t} = \nabla.(k\nabla T) + \rho_b c_b \omega_b (T_a - T) + Q_{met} \tag{7}$$

$$\rho_2 c_2 \frac{\partial T}{\partial t} = \nabla.(k\nabla T) + \rho_b c_b \omega_b (T_a - T) + Q_{met} + P \tag{8}$$

where ρ_1, ρ_2, and ρ_b represent the density of the tissue, tumor, and blood, respectively. c_1, c_2, and c_b are the specific heat capacities of the tissue, tumor, and blood, respectively. k is the thermal conductivity, T is the temperature, T_a is the arterial blood temperature, ω_b is the blood perfusion rate, Q_{met} is the metabolic heat

generation, and P represents the power dissipation of MNPs in the tumor.

To solve the Pennes bioheat equation, the boundary conditions were defined such that the heat flux is zero at the upper and lower boundaries $\left(\frac{\partial T}{\partial n} = 0\right)$, and the temperature on the body surface is maintained at 37 °C.

2.5. Fluid Modeling

The fluid flow in the bladder lumen is modeled using the Navier-Stokes equations with the Boussinesq approximation, which in the steady state are given by [19,20]:

$$\rho \nabla . (\vec{v}\vec{v}) = \mu \nabla^2 \vec{v} - \nabla p + \rho g \beta (T - T_0)\hat{e}_z \quad (9)$$

The left-hand side of this equation represents the change in the motion of a fluid element with velocity $\vec{v}$ and constant density ρ. The right-hand side of the equation describes the forces acting on the fluid element. The first term on the right-hand side represents the frictional forces between neighboring fluid elements, determined by the fluid's viscosity μ. The viscosity of urine was assumed to be 0.000824 Pa s [21]. The second term represents the pressure gradient, where p is the pressure. The third term represents the volumetric force acting on the fluid element, which derives convection, and includes gravitational acceleration g, density ρ, and the thermal expansion coefficient β. We used $T_0 = 37$ °C and $\beta = 3.61 \times 10^{-4}$ K^{-1} [22].

At the steady state $\left(\frac{\partial T}{\partial t} = 0\right)$, the heat equation for the fluid is given by:

$$-k\nabla^2 T + \rho c(\vec{v}.\nabla T) = 0 \quad (10)$$

where k, ρ, and c are the thermal conductivity, density, and specific heat capacity of urine, respectively. Similar to Equation (9), T represents the temperature, and $\vec{v}$ denotes the velocity of the fluid element. To solve the equations, the boundary conditions were defined such that the fluid velocity on the boundaries (the inner wall of the bladder and the surface of the tumor) is zero, $\vec{v} = 0$.

2.6. Numerical Solution and Simulation Setup

The finite element method (FEM) was employed to solve the equations. Figure 3 illustrates the mesh used for performing the calculations. The calculations were performed using a "free triangular" mesh. Due to the greater importance and intensity of temperature and heat variations in the bladder wall, bladder cavity, and tumor, a finer mesh was employed in these regions. Additionally, for the case involving convection, the "boundary layers" mesh was applied to the tumor wall and the inner wall of the bladder, both of which are in contact with urine and exposed to convective heat transfer. A mesh independence test was conducted for the studied quantities to ensure the accuracy and reliability of the numerical results. The results demonstrated that the solution for the studied quantities is independent of the mesh resolution, confirming that further refinement of the mesh does not significantly affect the outcome.

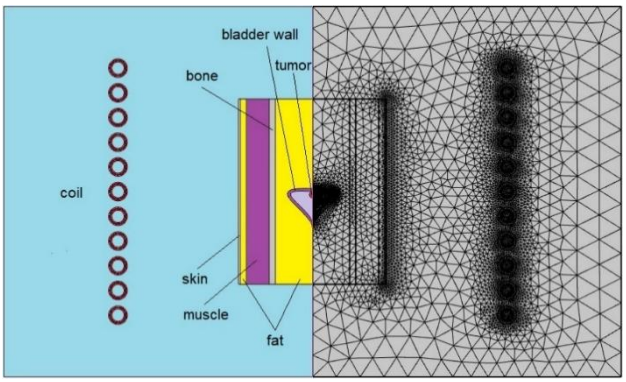

Fig. 3. Computational domain (left) and its mesh (right).

In this simulation, after injecting Fe_3O_4 MNPs into the tumor and achieving a uniform distribution and steady-state conditions, the target tissue is exposed to the AMF generated by the induction coil. To investigate the effect of urine on the simulation results of MNPs hyperthermia in bladder cancer, the calculations were performed for the following cases:

- Case 1: The bladder is assumed to be empty of urine, solid, and muscle-like.
- Case 2: Since the bladder is not empty during treatment, urine is considered to be present within the bladder cavity. The thermal properties of urine are incorporated into the simulation, while the blood perfusion rate ω_b and the metabolic heat generation Q_{met} in the bladder cavity, are set to zero. In this case, the effect of convection within the urine is neglected.
- Case 3: Inside the bladder cavity, urine is taken into account, similar to Case 2. In addition to the conditions of Case 2, the effect of convection within the urine is also considered in this case.

In Case 3, urine convection is assumed to result from temperature gradients induced by localized heating within the bladder tumor. Forced convection effects—such as those occurring during clinical bladder irrigation, where saline is introduced into the bladder at operator-dependent flow rates—are not considered in the model.

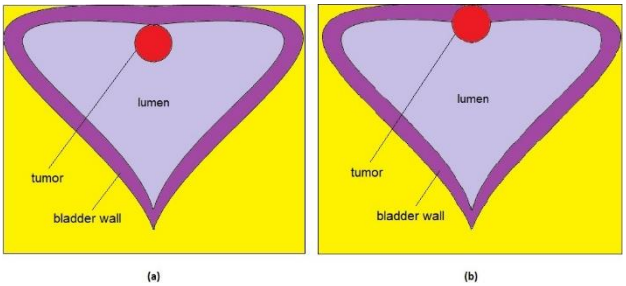

Fig. 4. Two stages of bladder cancer investigated in this study: (a) T1 and (b) T2.

Cases 1, 2, and 3 were conducted for two stages of bladder cancer (T1 and T2), as illustrated in Figure 4. To ensure computational efficiency and focus on key thermal effects, T1 NMIBC and T2 MIBC were modeled as spheres positioned at different depths relative to the bladder wall. This geometric simplification facilitates the isolation of urine and convection effects while aligning

with established practices in early-stage thermal modeling. Although anatomically simplified, the model serves as a practical foundation for preliminary analysis before more detailed, anatomically accurate simulations.

The volume used in the modeling for the bladder is 60 mL, which falls within the normal range for post-void residual urine volume. In Table 1, the dimensions of the geometry are provided, and in Table 2, the thermal properties of healthy tissues, the tumor, and urine are presented. Due to the lack of data on the thermal properties of bladder cancer, the properties of liver cancer were used as a substitute, since the thermal properties of non-cancerous liver and bladder tissues differ by less than 1.5 % [31,33].

Table 1
Geometry dimensions [23–25].

Property	Value (cm)
Bladder wall thickness	0.5
Tumor radius	0.5
Fat	6
Bone	1
Muscle	3.7
Subcutaneous fat	1
Skin	0.3
Outer radius of the coil	1.5
Inner radius of the coil	1
Distance between the coils and the central axis of the body	30

Table 2
Parameter values for the simulations [26–32].

Parameters	Blood	Skin	Bone	Fat	Bladder	Muscle	Tumor	Urine
c (J kg^{-1} K^{-1})	3770	3391	2274	2348	3581	3421	3581	4178
ρ (kg m^{-3})	1060	1109	1178	911	1086	1090	1086	1024
k (W m^{-1} K^{-1})	0.52	0.37	0.31	0.21	0.52	0.49	0.52	0.56
ω (s^{-1})	-	0.05	0.00014	0.00125	0.0014	0.00165	0.00165	0
Q_{met} (W m^{-3})	-	368.1	70	368.3	14414	684.2	72070	0

Table 3
Physical properties of Fe_3O_4 [17,34].

Parameters	Values
$\boldsymbol{D}$ (nm)	19
$\boldsymbol{\delta}$ (nm)	1
$\boldsymbol{\phi}$	0/071
$\boldsymbol{M_d}$ (kA m^{-1})	446
$\boldsymbol{K_{eff}}$ (kJ m^{-3})	9
τ_0 (s)	10^{-9}

The physical properties of Fe_3O_4 MNPs are presented in Table 3. The frequency used in the simulation is 100 kHz, and the electric current is 88 A.

It should be noted that this electric current value was determined in Case 1 by targeting the tumor within the therapeutic temperature range for destruction (41 °C and above) while ensuring the surrounding tissue remains within the permissible temperature range (below 45 °C). To ensure comparability of the simulation results, the electric current value in the other two simulation cases was also set to 88 A. Therefore, this electric current value may not be optimal for Cases 2 and 3. This choice was made to maintain identical AMF excitation across all cases, allowing us to isolate the specific effects of urine presence and convection on heat transfer, independent of variations in the electric current.

3. RESULTS AND DISCUSSION

In this section, we present the results obtained from the simulations. Specifically, the distribution of the volumetric heat generation rate due to induction heating, the distribution of the volumetric power dissipation of the MNPs, and the temperature distribution are analyzed for two stages of bladder cancer (T1 and T2) across three cases: the muscle-like bladder, the bladder with urine without convection, and the bladder with urine including convection.

3.1. Induction Heating in Healthy Tissue and Tumor

As previously mentioned, the AMF generated by the coil creates an electric field around it, which induces eddy currents in the workpiece (here, the human body). Due to the electrical resistance of the workpiece, Joule heating occurs. In this section, the distribution of the volumetric heat generation rate due to induction heating is presented for two stages of bladder cancer (T1 and T2) across the three cases mentioned above. Figure 5 illustrates the distribution of the volumetric heat generation rate in both healthy tissue and the tumor, while Figure 6 focuses on the distribution of the volumetric heat generation rate within the tumor itself.

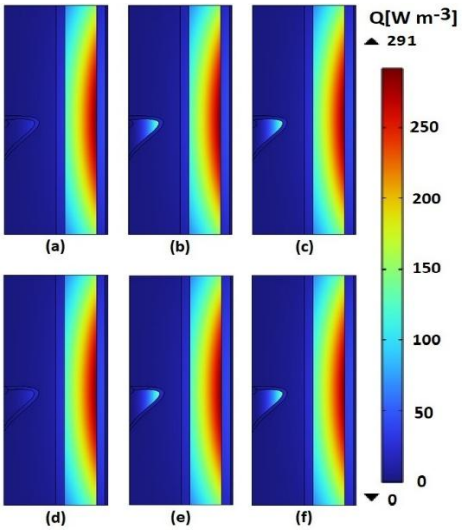

Fig. 5. Distribution of the volumetric heat generation rate due to induction heating in healthy tissue and tumor: (a) T1, muscle-like bladder; (b) T1, bladder with urine without convection; (c) T1, bladder with urine including convection; (d) T2, muscle-like bladder; (e) T2, bladder with urine without convection; (f) T2, bladder with urine including convection.

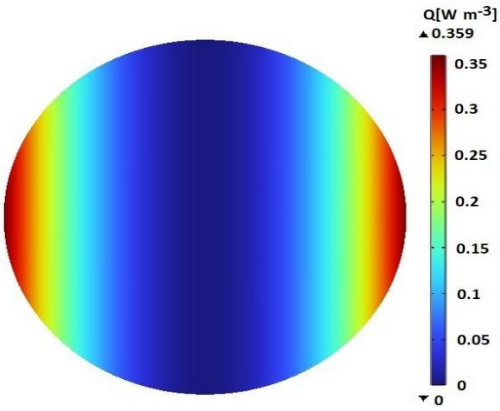

Fig. 6. Distribution of the volumetric heat generation rate due to induction heating within the tumor, for both stages of bladder cancer (T1 and T2), across all three cases.

As shown in Figure 5, the highest volumetric heat generation rate occurs in the muscle for both stages of bladder cancer and across all three cases considered. This is attributed to the higher electrical conductivity of muscle (0.362 S m^{-1}) compared to skin, fat, bone, and the bladder wall. As observed, the skin effect results in a decrease in volumetric heat generation rate from the tissue surface toward the center of the body [35]. For this reason, in Figures 5(a) and 5(d), where the bladder is modeled as muscle tissue, the volumetric heat generation rate inside the bladder remains low despite the high electrical conductivity of muscle. In Figures 5(b), 5(c), 5(e), and 5(f), the volumetric heat generation rate in the bladder increases due to the presence of urine. This increase is attributed to the higher electrical conductivity of urine (1.75 S m^{-1}) compared to that of muscle.

Figure 6 demonstrates that the volumetric heat generation rate in the tumor is similar for both T1 and T2 across all three cases, with its value being very small. It is also observed that the volumetric heat generation rate, influenced by the skin effect, is higher at the tumor's surface and decreases toward its center. It should be noted that the volumetric heat generation rate gradient in the tumor is independent of its shape and location, decreasing linearly toward the center.

3.2. Distribution of the Volumetric Power Dissipation of the MNPs

Since it is assumed that Fe_3O_4 MNPs are exclusively localized within the tumor, the distribution of the volumetric power dissipation of the MNPs (referred to as the volumetric heat generation rate of the MNPs) is observed only in the tumor. This localization helps minimize damage to healthy tissue. Figure 7 shows the distribution of the volumetric heat generation rate of the MNPs for two stages of bladder cancer (T1 and T2) across the three studied cases.

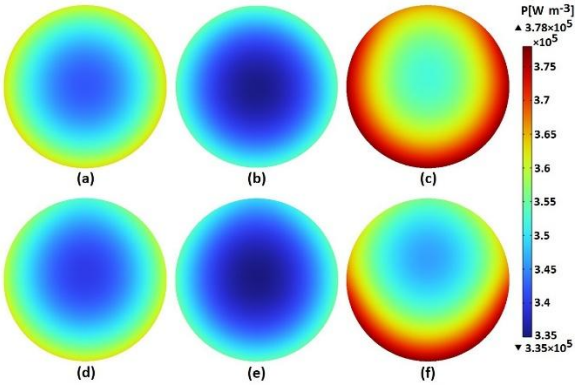

Fig. 7. Distribution of the volumetric heat generation rate of the MNPs within the tumor: (a) T1, muscle-like bladder; (b) T1, bladder with urine without convection; (c) T1, bladder with urine including convection; (d) T2, muscle-like bladder; (e) T2, bladder with urine without convection; (f) T2, bladder with urine including convection.

As observed, the volumetric heat generation rate of the MNPs is at its minimum at the center of the tumor and increases toward the periphery, reaching its maximum value at the tumor's surface. As shown in Figures 7(b) and 7(e), when urine is included in the model with perfusion absent within the bladder lumen but convection neglected (Case 2), the volumetric heat generation rate of the MNPs in the tumor is reduced compared to Figures 7(a) and 7(d), where the bladder is assumed to be devoid of urine and modeled as muscle tissue (Case 1). When convection in urine is considered (Case 3), as shown in Figures 7(c) and 7(f), the volumetric heat generation rate of the MNPs increases compared to Cases 1 and 2. This increase is observed in Case 3, particularly in the border regions of the tumor that are in contact with urine. Therefore, it is evident that convection within the bladder enhances the heat generation of the MNPs in the tumor.

The difference in the distribution of the volumetric heat generation rate of the MNPs across the three cases, for both stages of bladder cancer, is due to the dependence of the volumetric heat generation rate of the MNPs on changes in temperature and magnetic field (see Subsection 2.3). Since the magnetic field for a specific tumor is the same across

the three cases, the results indicate that the temperature distribution varies across the three modeled cases for a specific tumor, as discussed in the next subsection. It should be noted that the magnetic field distribution in T1 and T2 differs due to the variation in tumor location relative to the induction coil.

By comparing Figures 6 and 7, it is evident that the volumetric heat generation rate due to induction heating in the tumor is significantly lower than the volumetric heat generation rate of the MNPs. According to calculations, the volumetric heat generation rate due to induction heating in the tumor is 10^{-4} % of the volumetric heat generation rate of the MNPs ($Q=1.4354\times10^{-1}$ W m^{-3} and $P=4.6529\times10^{5}$ W m^{-3}). Therefore, the heat generation of the MNPs can be considered the total heat generation.

3.3. Temperature Distribution in Healthy Tissue and Tumor

As mentioned, to investigate heat transfer and determine the temperature distribution, Pennes bioheat equation (Equations (7) and (8)) is applied to solid tissues, while the Navier-Stokes and heat equations (Equations (9) and (10)) are used for the fluid domain (in Case 3). Figure 8 shows the temperature distribution in both healthy tissue and the tumor, while Figure 9 shows the temperature distribution specifically within the tumor.

As can be seen, the temperature is highest at the center of the tumor and decreases as it moves away from the center (due to heat transfer from the surrounding area). The temperature in the areas far from the tumor is 37 °C. A slight increase in temperature is observed around the tumor in the bladder, but it does not harm the healthy tissue, as the temperature remains below 45 °C [10,11]. This is the desirable feature of MNPs hyperthermia, which localizes the heat and prevents damage to the surrounding tissue. It can be seen that the distribution pattern of the volumetric heat generation rate of the MNPs, as shown in the previous subsection, is inversely related to the temperature distribution pattern in the tumor. In contrast to the temperature distribution, the lowest heat generation occurs at the center of the tumor, while the highest heat generation occurs at the tumor's surface. This contrast corresponds to the inverse square relationship between the volumetric heat generation rate of the MNPs and temperature, as derived from Equation (2).

Figures 8(a), 8(d), 9(a), and 9(d) show the case where the bladder is void of urine and is entirely solid (muscle-like). Therefore, all heat transfer calculations were performed using the Pennes equation (Case 1). In this case, perfusion in the muscle-like bladder causes cooling. Figures 8(b), 8(e), 9(b), and 9(e) illustrate the case where urine is present inside the bladder but convection is neglected, with calculations performed using the Pennes equation (Case 2). In this case, it can be observed that the temperature field in the tumor and its surrounding tissue has increased compared to Case 1. This increase in temperature field is due to the absence of perfusion within the bladder lumen. Therefore, considering the presence of urine without convection within the bladder and the absence of perfusion, the temperature distribution changes, showing an increase in the temperature field. Figures 8(c), 8(f), 9(c), and 9(f) show the case where the effect of convection in the bladder containing urine is taken into account. Therefore, the Navier-Stokes and heat equations for fluid were used in the calculations (Case 3). In this case, it can be observed that the temperature distribution has changed compared to the previous cases, resulting in a decrease in the temperature field relative to Cases 1 and 2. The decrease in the temperature field is due to the presence of convection within the urine and its cooling effect on the tumor and its surrounding tissues. Accordingly, the decrease in temperature caused by convection within the urine dominates the increase in temperature resulting from the absence of perfusion within the bladder lumen. Thus, when urine convection was included, the simulations showed a reduced tumor temperature but an increased volumetric heat generation rate of the MNPs (see Subsection 3.2). This paradox arises because cooling by convection increases the magnetic susceptibility and relaxation times, which enhances heating efficiency (see Equation (2)), while the stronger advective heat removal dominates, leading to a lower overall tumor temperature. Since convection increases heat removal from the tumor, greater MNP heat generation is required to maintain therapeutic temperatures.

In Figures 9(c) and 9(f), it can be observed that the temperature of the part of the tumor directly adjacent to the urine has decreased due to the presence of convection, compared to the temperature of the same areas in Cases 1 and 2. By examining Figure 8, the maximum temperature values at the center of the tumor can be compared across the three studied cases for each stage of bladder cancer. The temperature at the center of the tumor in T1 for Cases 1, 2, and 3 is 44.6, 45.6, and 43 °C, respectively, and in T2 for Cases 1, 2, and 3, it is 44.9, 45.7, and 44 °C, respectively. Therefore, the maximum temperature value in both T1 and T2 is highest in Case 2 and lowest in Case 3. This result is consistent with the results and arguments of the previous paragraph.

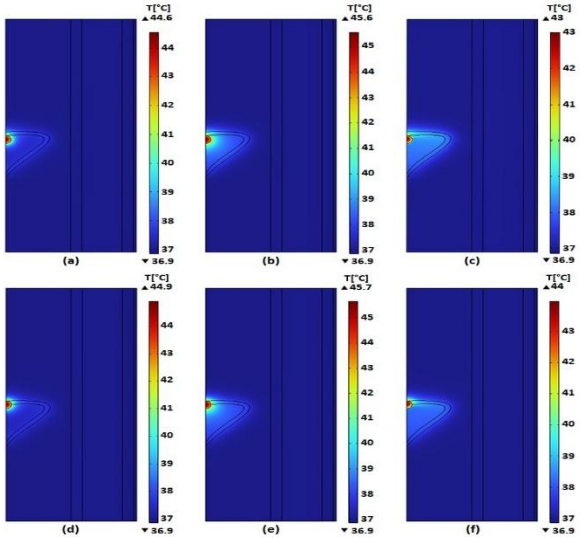

Fig. 8. Temperature distribution in healthy tissue and the tumor: (a) T1, muscle-like bladder; (b) T1, bladder with urine without convection; (c) T1, bladder with urine including convection; (d) T2, muscle-like bladder; (e) T2, bladder with urine without convection; (f) T2, bladder with urine including convection.

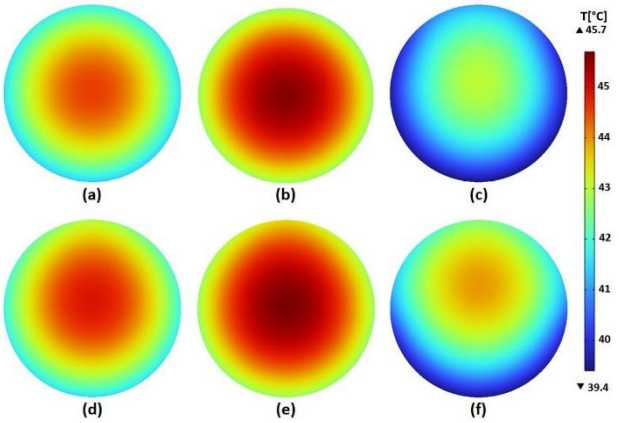

Fig. 9. Temperature distribution within the tumor: (a) T1, muscle-like bladder; (b) T1, bladder with urine without convection; (c) T1, bladder with urine including convection; (d) T2, muscle-like bladder; (e) T2, bladder with urine without convection; (f) T2, bladder with urine including convection.

To examine and compare the results more closely, Figure 10 presents the line graph of the temperature distribution on the tumor surface for T1 and T2 across the three simulated cases.

Line graphs indicate that, as you move along the tumor surface from point 1 to point 2, the temperature distribution curve in Case 1 is lower than in Case 2 for both T1 and T2. In Case 2, the temperature distribution curve shifts upward due to the absence of perfusion within the bladder lumen. Additionally, the temperature distribution becomes more uniform, particularly in areas adjacent to the urine. This uniformity in temperature distribution on the tumor surface is particularly noticeable in T1, as a larger portion of the tumor surface is adjacent to the urine. In Case 3, the temperature distribution curve shifts downward relative to Cases 1 and 2, owing to the convection within the urine and its associated cooling effect, which is evident in both T1 and T2. Thus, the temperature reduction induced by convection is greater than the temperature rise caused by the absence of perfusion.

In Case 3, the curve rises with a relatively steep slope as it moves along the tumor surface from point 1 to point 2 toward the bladder wall, a trend observed in both T1 and T2. As it approaches the bladder wall, the effect of convection diminishes and is eliminated in areas where the tumor is no longer in contact with the urine, resulting in an increase in temperature. Consequently, the temperature distribution in Case 3 exhibits greater non-uniformity.

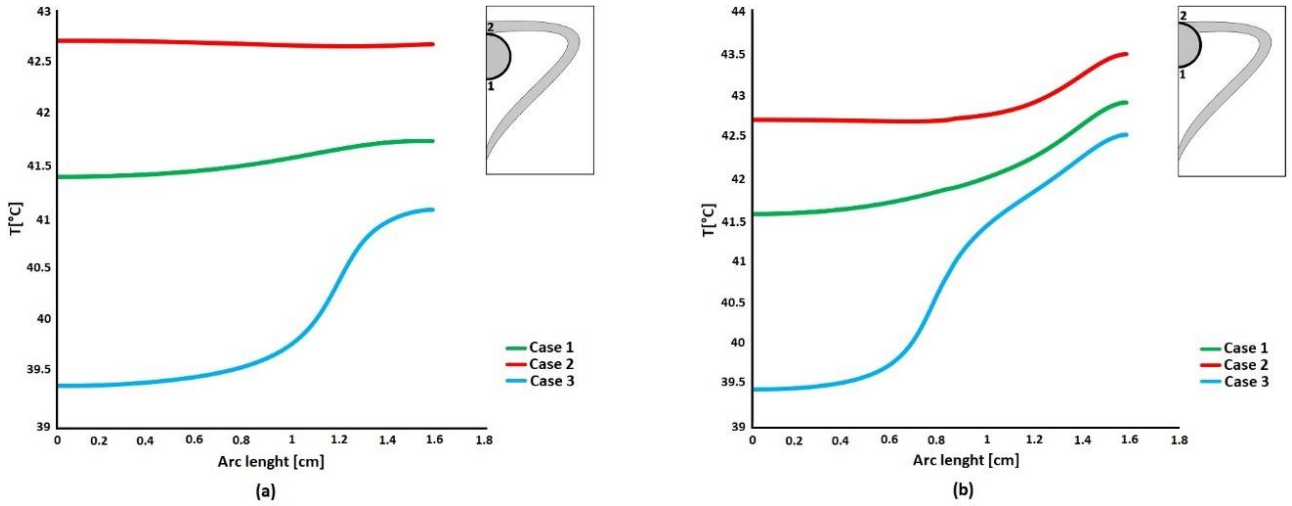

Fig. 10. Line graph of temperature distribution on the tumor surface (arc length): (a) T1, three cases and (b) T2, three cases.

In Figures 8, 9, and 10, it is evident that in each case, the temperature field in T1 is lower than in T2, and its distribution is more uniform. This result occurs because a larger portion of T1 is in the vicinity of urine and exposed to convection, whereas T2 extends into the bladder wall, with a smaller part near the urine.

The urine flow within the bladder is characterized as laminar. Figure 11 illustrates the streamlines of urine flow. Streamlines are curves tangent to the velocity vectors at every point in the fluid, representing the instantaneous direction of flow. As observed, the density of the streamlines is higher near the tumor (heat source) and decreases with increasing distance from these regions. The direction of the streamlines, indicated by the red arrows, demonstrates that the area of urine adjacent to the tumor flows upward in the bladder due to the rise in temperature and subsequent decrease in density. As a result, urine with a lower temperature and higher density moves downward. These displacements create a large convection cell in the upper region of the bladder, adjacent to the tumor, which extends into the bladder walls. A smaller counter-rotating cell also forms at the base of the bladder due to the change in geometry and flow separation.

These convective flows persist throughout the treatment and continue as long as the tumor's temperature remains higher than that of the surrounding tissue. As observed, the presence of convection in the urine leads to a decrease in the temperature of both the tumor and the surrounding tissue.

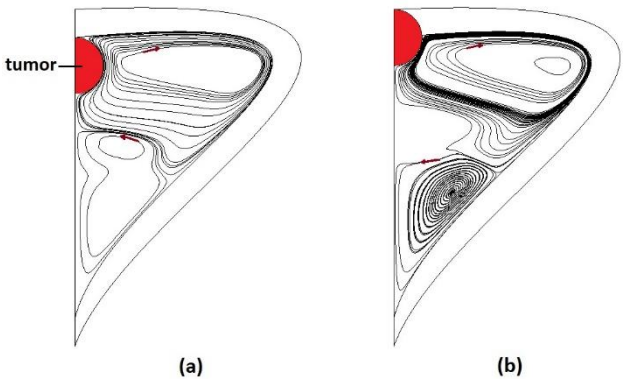

Fig. 11. Urine streamlines (velocity field) within the bladder, with marked tumor location: (a) T1 and (b) T2.

3.4. Limitations and Future Work

This study has several limitations that should be acknowledged. The tumor was modeled as spherical with a uniform nanoparticle distribution, and the computational system was represented using a 2D axisymmetric geometry. These simplifications reduced computational cost and allowed clearer interpretation of the effects of urine presence and convection, but future work will extend the model to irregular tumor geometries, heterogeneous nanoparticle distributions, and full 3D domains to capture more anatomical detail and improve clinical relevance. While the focus was on the physical aspects of MNP heating, thermal dose metrics such as CEM43 and Arrhenius-based damage integrals, which are essential for quantifying biological effects, were not included and will be incorporated in future work to extend the modeling toward treatment outcome evaluation. Finally, the study was purely numerical due to the challenges of experimentally controlling urine convection. Nevertheless, the Pennes and Navier-Stokes framework used here is well established, and our results are consistent in both temperature ranges and trends with previously reported hyperthermia studies [2,12,15].

4. CONCLUSION

In this article, the effect of urine and its convection within the bladder on MNPs hyperthermia in bladder cancer was investigated. For this purpose, a numerical study was conducted on the MNPs hyperthermia process using Fe_3O_4 nanoparticles in two stages of bladder cancer (T1 and T2) in three cases. While this study focused on a spherical tumor at a specific location, the methodology and findings may provide insights applicable to non-spherical tumor shapes and other tumor locations, subject to further validation. The results indicated:

- The presence of urine does not affect the heat generated by induction heating in the tumor, but increases it within the bladder cavity (inside the urine).
- The heat generated by the MNPs, which is localized within the tumor in this hyperthermia method, is at its minimum at the center of the tumor and increases toward the periphery, reaching its maximum value at the tumor's surface. The convection within the urine enhances the heat generation of the MNPs in the tumor.
- The temperature is highest at the center of the tumor and decreases as it moves away from the center.
- The absence of perfusion within the bladder lumen increases the temperature and improves its uniformity within the tumor.
- The convection within urine causes a decrease in temperature in the tumor and surrounding healthy tissue. Additionally, the presence of convection results in a more non-uniform temperature distribution within the tumor.
- The effect of decreasing the temperature due to convection within urine is more dominant than the effect of increasing the temperature due to the absence of perfusion within the bladder lumen.
- The temperature distribution in T1 is more uniform than in T2, so it seems that MNPs hyperthermia is more effective in treating NMIBC than MIBC.

As expected and confirmed by the results, in the MNPs hyperthermia, the localized heat generation maintains the temperature in the surrounding healthy tissue within a safe range. Therefore, the cooling effect of urine is unnecessary for the surrounding tissue. As a result, it can be concluded that the cooling effect of urine in this hyperthermia method lowers the temperature of the tumor, thereby diminishing the treatment's effectiveness. To offset the temperature-reducing influence of urine on the tumor's temperature, the input electric current in the coil can be increased. This would raise the tumor's temperature and maintain the treatment's efficacy. Therefore, given the significant influence of urine and its convective properties on temperature distribution, it is essential to account for the presence of urine and its convection within the bladder when conducting simulations related to MNPs hyperthermia for bladder cancer. This consideration will enable more accurate predictions of experimental outcomes and improve the reliability of the treatment planning process.

ACKNOWLEDGEMENT

This research was supported by Bu-Ali Sina University under grant No. 1002763.

CONFLICTS OF INTEREST

The authors declare that there are no conflicts of interest regarding this article.

REFERENCES

[1] Stauffer, P. R. and van Rhoon, G. C., Overview of bladder heating technology: matching capabilities with clinical requirements, Int. J. Hyperthermia, 2016, 32 (4), 407–416.

[2] Schooneveldt, G., Kok, H. P., Bakker, A., et al., Clinical validation of a novel thermophysical bladder model designed to improve the accuracy of hyperthermia treatment planning in the pelvic region, Int. J. Hyperthermia, 2018, 35 (1), 383–397.

[3] Duan, H., Deng, Z., Zou, J., Zhang, G., Zou, X. and Xie, T., The efficacy and safety of hyperthermia intravesical chemotherapy in the treatment of non-muscle-invasive bladder cancer: a meta-analysis, Urol. Int., 2024, 108 (4), 322–333.

[4] Melgarejo Segura, M. T., Yanez Castillo, Y., Lozano Lorca, M., Morales Martinez, A., Arrabal Polo, M. A.

and Arrabal Martin, M., Efficacy of conduction hyperthermia in the treatment of non-muscle invasive bladder cancer: a systematic review, Urol. Oncol., 2024, 42 (9), 251–265.

[5] Akdas, E. M., Culha, M. M., Telli, E., et al., The effect of intravesical chemohyperthermia with mitomycin in non-muscle-invasive bladder tumour patients who cannot tolerate BCG treatment or recur after treatment and refuse cystectomy, Int. Urol. Nephrol., 2025, 57 (1), 63–69.

[6] Riesterer, O., Ademaj, A., Puric, E., et al., Tetramodal therapy with transurethral resection followed by chemoradiation in combination with hyperthermia for muscle-invasive bladder cancer: early results of a multicenter phase IIB study, Int. J. Hyperthermia, 2022, 39 (1), 1078–1087.

[7] Ademaj, A., Puric, E., Marder, D., et al., Radiotherapy combined with deep regional hyperthermia in elderly and frail patients with muscle-invasive bladder cancer: quality analysis of hyperthermia and impact on clinical results, Int. J. Hyperthermia, 2023, 40 (1), 1–9.

[8] Tsai, T. F., Hwang, T. I., Chen, P. C., et al., Hyperthermia reduces cancer cell invasion and combats chemoresistance and immune evasion in human bladder cancer, Int. J. Oncol., 2024, 65 (6), 116.

[9] Hedayatnasab, Z., Abnisa, F. and Daud, W. W., Review on magnetic nanoparticles for magnetic nanofluid hyperthermia application, Mater. Des., 2017, 123, 174–196.

[10] Stoll, A. M. and Greene, L. C., Relationship between pain and tissue damage due to thermal radiation, J. Appl. Physiol., 1959, 14 (3), 373–382.

[11] Kok, H. P., Korshuize-van Straten, L., Bakker, A., et al., Online adaptive hyperthermia treatment planning during locoregional heating to suppress treatment-limiting hot spots, Int. J. Radiat. Oncol. Biol. Phys., 2017, 99 (4), 1039–1047.

[12] Oliveira, T. R., Stauffer, P. R., Lee, C. T., et al., Magnetic fluid hyperthermia for bladder cancer: A preclinical dosimetry study, Int. J. Hyperthermia, 2013, 29 (8), 835–844.

[13] Yuan, Y., Cheng, K. S., Craciunescu, O. I., et al., Utility of treatment planning for thermochemotherapy treatment of nonmuscle invasive bladder carcinoma, Med. Phys., 2012, 39 (3), 1170–1181.

[14] Sadee, C. and Kashdan, E., A model of thermotherapy treatment for bladder cancer, Mathematical Biosciences and Engineering (MBE), 2016, 13 (6), 1169–1183.

[15] Ooi, E. H., Popov, V., Alfano, M. and Cheong, J. K. K., Influence of natural convection on gold nanorods-assisted photothermal treatment of bladder cancer in mice, Int. J. Hyperthermia, 2020, 37 (1), 634–650.

[16] Heidari, H., Tavakoli, M. H., Shokri, A., Mohamad Moradi, B., Mohammad Sharifi, O. and Asaad, M. J. M., 3D simulation of the coil geometry effect on the induction heating process in Czochralski crystal growth system, Cryst. Res. Technol., 2020, 55 (3), 1900147.

[17] Rosensweig, R. E., Heating magnetic fluid with alternating magnetic field, J. Magn. Magn. Mater., 2002, 252, 370–374.

[18] Tang, Y., Jin, T., Flesch, R. C. C., and Gao, Y., Improvement of solenoid magnetic field and its influence on therapeutic effect during magnetic hyperthermia, J. Phys. D: Appl. Phys., 2020, 53 (30).

[19] Anderson, J. D., Governing equations of fluid dynamics. In: Wendt, J. F. editor, Computational fluid dynamics, Springer, Berlin, Heidelberg, 1992, 15–51.

[20] Gomez-Blanco, J. C., Martinez-Reina, F. J., Cruz, D., Pagador, J. B., Sanchez-Margallo, F. M. and Soria, F., Fluid structural analysis of urine flow in a stented ureter, Comput. Math. Methods Med., 2016, 2016, 5710798.

[21] Inman, B. A., Etienne, W., Rubin, R., et al., The impact of temperature and urinary constituents on urine viscosity and its relevance to bladder hyperthermia treatment, Int. J. Hyperthermia, 2013, 29 (3), 206–210.

[22] Kell, G. S., Density, thermal expansivity, and compressibility of liquid water from 0° to 150°C: correlations and tables for atmospheric pressure and saturation reviewed and expressed on 1968 temperature scale, J. Chem. Eng. Data., 1975, 20 (1), 97–105.

[23] Jequier, S. and Rousseau, O., Sonographic measurements of the normal bladder wall in children, AJR Am. J. Roentgenol., 1987, 149 (3), 563–566.

[24] Bi, X., Loo, Y. T. and Henry, C. J., Ultrasound measurement of intraabdominal fat thickness as a predictor of insulin resistance and low HDL cholesterol in Asians, Nutrition, 2018, 55–56, 99–103.

[25] Wang, S., Yu, R. X., Fan, W., et al., Detection of skin thickness and density in healthy Chinese people by using high-frequency ultrasound, Skin Res. Technol., 2023, 29 (1), e13219.

[26] Xu, F., Seffen, K. A. and Lu, T. J., Non-Fourier analysis of skin biothermomechanics, Int. J. Heat. Mass. Tran., 2008, 51 (9--10), 2237–2259.

[27] Adhikary, K. and Banerjee, M., A thermofluid analysis of the magnetic nanoparticles enhanced heating effects in tissues embedded with large blood vessel during magnetic fluid hyperthermia, J. Nanopart., 2016.

[28] Bousselham, A., Bouattane, O., Youssfi, M. and Raihani, A., Brain tumor temperature effect extraction from MRI imaging using bioheat equation, Procedia. Comput. Sci., 2018, 127, 336–343.

[29] Dimitriou, N. M., Pavlopoulou, A., Tremi, I., Kouloulias, V., Tsigaridas, G. and Georgakilas, A. G., Prediction of gold nanoparticle and microwave-induced hyperthermia effects on tumor control via a simulation approach, Nanomaterials, 2019, 9 (2), 167.

[30] Kandala, S. K., Sharma, A., Mirpour, S., Liapi, E., Ivkov, R. and Attaluri, A., Validation of a coupled electromagnetic and thermal model for estimating temperatures during magnetic nanoparticle

hyperthermia, Int. J. Hyperthermia, 2021, 38 (1), 611–622.
[31] Cheong, J. K. K., Ooi, E. H., Chiew, Y. S., et al., Gold nanorods assisted photothermal therapy of bladder cancer in mice: a computational study on the effects of gold nanorods distribution at the center, periphery, and surface of bladder cancer, Comput. Methods. Programs. Biomed., 2023, 230, 107363.
[32] Baumgartner, C., Hasgall, P. A., Gennaro, F. D., et al., IT'IS Database for thermal and electromagnetic parameters of biological tissues, [cited 2024]. Available from: itis.swiss/database
[33] Wright, N. T., On a relationship between the Arrhenius parameters from thermal damage studies, J. Biomech. Eng., 2003, 125 (2), 300–304.
[34] Maenosono, Sh. and Saita, S., Theoretical assessment of FePt nanoparticles as heating elements for magnetic hyperthermia, IEEE Trans. Magn., 2006, 42 (6), 1638–1642.
[35] Rudnev, V., Loveless, D. and Cook, R. L., Handbook of induction heating, CRC Press, 2017.